CDF/DOC/EXOTIC/INTERNAL/8979
Draft 1.3
February 20, 2008

Search for new physics in the exclusive $\gamma + \not\!\!E_{\rm T}$ final state.

Max Goncharov[1]
Texas A&M University
V. Krutelyov
UCSB
R. Culbertson, A. Pronko
Fermilab

Abstract

The photon plus missing transverse energy signal is comparatively rare in the Standard Model. The production is dominated by the electroweak $\mathrm{Z}+\gamma$ process. This signature is a sensitive place to search for new high-energy invisible particles because photons, radiated by incoming partons in a collision, can be the only tag available to us in the detection of such processes. Photons are also good candidates to be produced in the decay chains of new particles and appear in such popular models as Large Extra Dimensions.

This note presents the search for physics beyond the Standard Model in the exclusive $\gamma+\not\!\!E_{\rm T}$ channel using 2 fb^{-1} of data collected by the CDFII detector. The observed number of events is consistent with background expectations. We set upper limits on the mass of KK graviton for a range of extra dimensions in Large Extra Dimensions models. We also combine this result with the recently updated search in the exclusive $Jet + \not\!\!E_{\rm T}$ channel.

[1]maxi@fnal.gov

Contents

1 Introduction

This note describes a search for physics beyond the Standard Model in the exclusive γ+$\not\!\!E_{\rm T}$ final state. It is designed as a signature based search. First we estimate the backgrounds for the photon $E_{\rm T}$> 50 GeV, and then look at the data. In the end we select the optimal cut on the photon $E_{\rm T}$ to gain the best sensitivity for Large Extra Dimensions (LED) model.

The note starts with motivation for this analysis and why this signature is interesting and important. Next, data selection and topological cuts are described. After that we estimate the signal efficiency and describe the dominant backgrounds. At the end we determine 95% C.L. limits for the LED model for 2, 3, 4, 5, and 6 extra dimensions. We also specify a general method for comparing theoretical predictions to this data, and find an upper limit of 14.3 events from new physics, which is equivalent to an upper limit on cross-section of 14.4 ± 1.5 fb^{-1} for beyond the Standard Model processes.

The most dominant background comes from cosmic rays, therefore we start the background section with the description of cosmic ray background and methods/cuts we use to reduce it. Then we turn to the backgrounds from the Standard Model (SM), most of which arise from Electroweak or QCD processes when one of the high $P_{\rm T}$ objects is lost. Most of the backgrounds are estimated from data using $W \rightarrow e\nu$ events.

2 Theoretical Motivation

Many extensions of the SM predict the existence of minimally-interacting particles, such as Kaluza-Klein (KK) states of the graviton in models with Large Extra Dimensions [1] or the gravitino in Supersymmetric models. Such particles would leave the detector unobserved and the only trace of their production can be inferred from a presence of the large transverse missing energy in those events.

Photons can appear in the final state because of two reasons: either they come from initial state radiation of charged quarks or they are directly produced in association with particles that escape undetected [2]. Therefore this search in the γ+$\not\!\!E_{\rm T}$ final state explores a wide range of models and nicely complements the search in the monojet channel [3].

The main process that we target in the analysis is the LED production $q\bar{q} \rightarrow \gamma G_{KK}$. In this model extra spatial dimensions are assumed to be compactified with radius R. The model introduces the fundamental mass scale M_D. Those two parameters, M_D and R, are related to the Newton's constant and the number of extra dimensions by $G_N^{-1} = 8\pi R^n M_D^{2+n}$. The SM fields propagate only on the normal 3+1 dimensional plane, while gravitons propagate in the bulk, and would appear to us as massive states of the graviton, or, said differently, as massive minimally-interacting particles. Large values of R result in a large phase space for graviton production, canceling the weakness of the coupling to standard model fields. For a given number of extra dimensions

the production cross section scales as $1/M_D^{n+2}$. It turns out that the kinematics are independent of M_D for a given n.

Another process that we do not focus on here is $q\bar{q} \to \tilde{G}\tilde{G}\gamma$ production [4]. In this model the gravitino $\tilde{G}$ is the LSP. Other Superpartners are too heavy to produce on-mass-shell at the Tevatron energies. As a result of our search it is possible to set an absolute lower limit on the gravitino mass $m_{3/2}$ or, equivalently, the Supersymmetry breaking scale[2] $\sqrt{|F|}$. The production cross-section scales as $1/|F|^4$. The kinematic distributions are independent of $|F|$.

And at last, but not the least, this signature is sensitive to $Z\gamma$ production in case $Z \to \nu\nu$. The results of this search can also be used to explore anomalous couplings.

3 Data Selection

The analysis uses 1996 fb^{-1} of data collected with W_NOTRACK trigger. Good run version 17 for photons is used. All data is processed with GEN6 reconstruction [3] For the photon or electron selection we apply standard photon/electron ID cuts [5].

As we will later, the crucial part is rejecting cosmic ray backgrounds. EMTiming system [6] is crucial for that, unfortunately it was installed only after first 427 pb^{-1} were collected. Therefore the data set is logically divided into two periods: before the run 190851 when EMTiming system came fully online, and after that. First data period spans 427 pb^{-1} of data, and the second period - 1569 pb^{-1}. The last run number is 237795. For the first period of data the timing system on the hadronic calorimeter (HADTiming) is used. As a result some of the cuts have different efficiencies for the first and second data periods.

The goal of the analysis is to select events with a single high $E_{\rm T}$ photon and no other high $E_{\rm T}$ objects. Table 1 lists all topological cuts. Cuts 3, 4, and 7 are to reject cosmic ray background and described in detail in Section 4.

When we count tracks, we want to count only well measured tracks reconstructed in COT. A track is accounted for only if it passes pass the requirements listed in Table 2.

In the future, we would like to expand our rapidity coverage to include forward region. There are no photons from cosmics or beam halo background sources. As a result, the is no need for cosmic rejection cuts. However, at the moment there is no lepton to photon fake rate for the forward region which is crucial for the background estimates.

[2] $|F| = \sqrt{3} m_{3/2} M_P$

[3] The 0d part of bhelbd was gen5 production, but ntupled in GEN6. Due to the extensive remake during ntupling, everything except SVX and COT pattern recognition is GEN6.

1	Photon $E_{\rm T}$> 50 GeV	
2	$\not\!\!E_{\rm T}$> 50 GeV	
3	Photon is in time	$\lvert t_{em}\rvert < 3.14$ ns or $\lvert t_{had}\rvert < 8.8$ ns
4	Photon passes cosmic rejection cut:	$\rm P_{RVM} > 0.75$
5	No tracks with $P_{\rm T}$> 10 GeV	
6	No jets with $E_{\rm T}$> 15 GeV	
7	At least 3 COT tracks	
8	Beam halo rejection cut	nEmTowers > 8 and nHadTowers > 1

Table 1: Event topology cuts

Track $P_{\rm T}$> 0.3 GeV
COT Axial(Nhits>4) > 1
COT Stereo(Nhits>4) > 1
$\lvert d_0\rvert < 0.1$ cm

Table 2: Track selection cuts.

4 Non-Collision Backgrounds

This section deals with cosmic rays. This background, if left alone, would make the analysis impossible. There are three cuts, all listed in Table 1, that are designed to reject as much cosmics as possible and at the same time to be efficient for collision photons. All cuts to reject cosmics are chosen to optimize sensitivity for the second period (1.6 fb^{-1}) of data.

Reference [7] has all the information to understand cosmic and beam halo backgrounds, as well as methods that can employed to reduce/estimate them.

4.1 Timing Resolution and Efficiency

Figure 1 shows the time of arrival for electrons above 50 GeV from $W \to e\nu$ sample. In one case the EMTiming system is used, and in the other the HADTiming is used. The latter case relies on the fact that for high E_{T} electrons or photons part of the shower reaches the hadronic part of the calorimeter and deposits enough energy to trigger the timing readout. For both systems the optimal value of the timing cut is selected to be at 2σ, where σ is the system resolution. The important point is that HADTiming system is not as efficient in rejecting cosmics as EMTiming simply because the resolution for HADTiming is much worse.

Not every high E_{T} electron or photon deposits enough energy in the hadronic portion of the calorimeter, therefore HADTiming system is more and more inefficient as the energy of the electron or photon decreases. Figure 2 illustrates the point. While the EMTiming efficiency is flat as a function of E_{T}, the HADTiming efficiency is energy dependent. This is the main reason behind separating whole data into two sets. For the first portion, where HADTiming is used, the predicted number of events is convoluted with the shape from Figure 2.

In principal, photons and electrons start showering at the different depths. We use a sample of electrons from $W \to e\nu$ and photons from $\gamma +$ jet samples to find out by how much it affects the timing efficiency. We found that the difference is negligible and well covered by the systematic uncertainty of 2.2 % that arises from comparing electron and $\gamma +$ Jet samples in the next section.

4.2 Relevance Vector Machine

Requiring photons to be in time with the collision reduces cosmic background by a factor of ~ 15. Unfortunately this is not enough, there are still more photons from cosmics than from collision photons. Most of the work here is based on [7]. The implementation of RVM[4] is described in [8]. To train the discriminant, photons above 50 GeV are selected. The cosmic sample is comprised of photons in [30,80] ns window, and the collision photons are selected from $2 \times \sigma^{EMT}$ window plus a jet with $E_{\text{T}}>$

[4]Strictly speaking, Support Vector Machine is an absolute classifier. Here we use Relevance Vector Machine that outputs the probability for any event to be signal or background.

40 GeV. With the jet requirement the cosmic contamination of the collision sample is less than 1%. Both datasets are divided randomly into two halves. First one used to train RVM, and second one is used to cross-check the results. Three variables are used in discriminator: $\Delta\phi$ between a photon and a muon stub closest to the photon, ratio of the hadronic to electromagnetic energy for the photon (HadE/EmE), and ratio of the energy in CES to the electromagnetic energy of the photon.

After training, we apply results to the test sample and plot the rejection power vs. efficiency, shown on Figure 3. We select the cut at 0.75 as it provides the maximum sensitivity for the collision photons over cosmics. The efficiency is also cross-checked

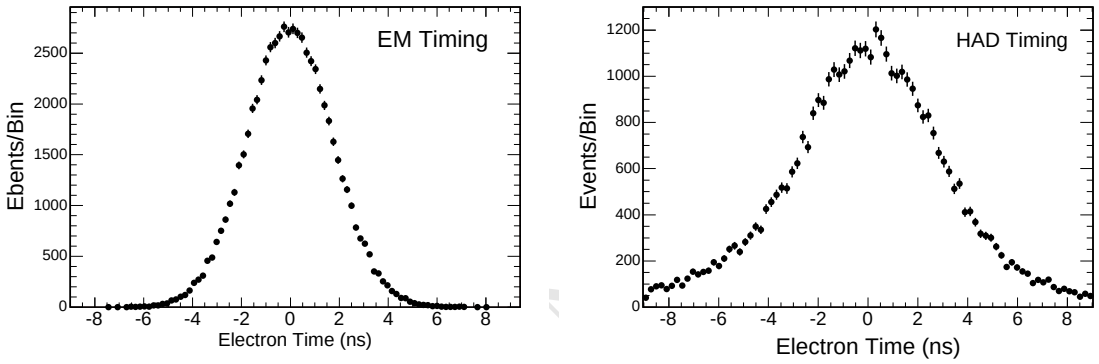

Figure 1: The figure shows the timing RMS for the electromagnetic and hadronic central calorimeters. The RMS for the electromagnetic part is clearly dominated by the collision RMS∼1.3 ns, while the RMS for the hadronic one is dominated by the timing resolution.

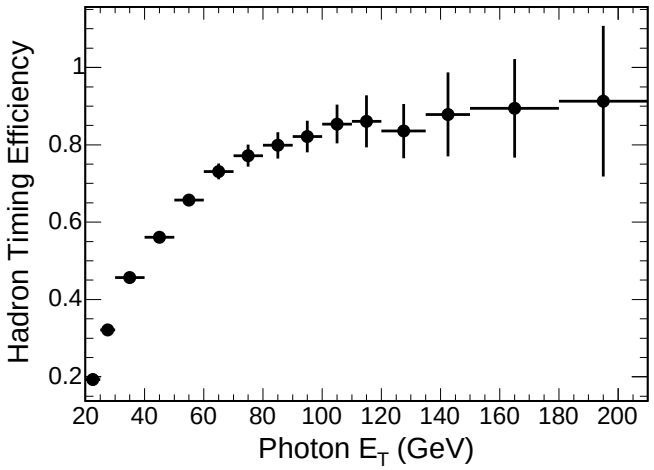

Figure 2: The efficiency of the hadronic timing as a function of photon E_{T} for the first data period. $W \rightarrow e\nu$ sample is used.

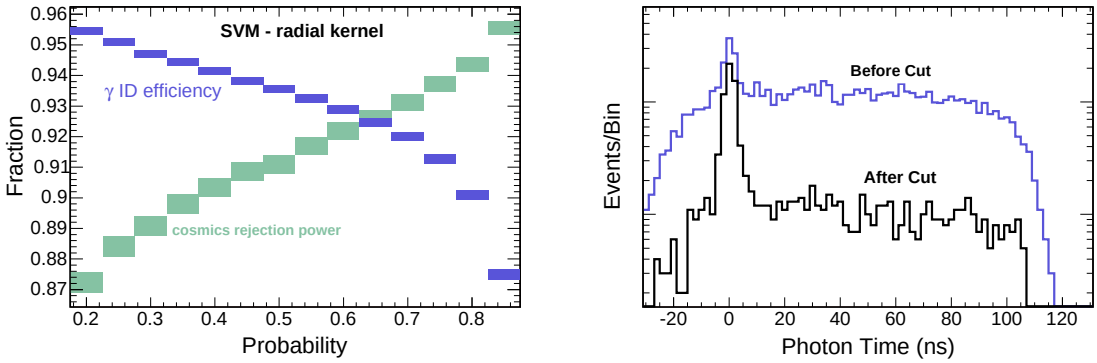

Figure 3: The left plot shows the photon efficiency and cosmic rejection power as a function of the SVM output. The cut at 0.75 gives the maximum sensitivity to collision photons. The plot on the right illustrates cosmic contamination before and after applying the SVM cut.

against electrons from $W \rightarrow e\nu$ sample. The efficiency is found to be independent of $E_{\rm T}$ for photons with $E_{\rm T}$> 40 GeV.

One important point to stress is that the signal efficiency is different for the first and second portions of data. The RVM uses HadE/EmE, the same variable that is responsible for triggering HADTiming system for the first set of data. In order to trigger hadronic timing the hadronic portion of a shower have to be significant. As a result it pushes signal efficiency for RVM from 91% to 95% for the first 427 pb^{-1}.

4.3 Cosmic Rays Background

The RVM discriminator reduces the cosmic background by another factor of ∼10. We reduce the cosmic background even further by asking that there are at least 3 COT tracks present in the events. Figure 4 shows the photon timing distribution before and after applying the cut on the number of tracks. It helps to reduce cosmics by another factor of ~ 3.

At the end, all 3 cuts on the photon timing, likelihood probability, and number of tracks reduce cosmic background by a factor of ~ 600. To estimate what the remaining background looks like, we apply all of the analysis cuts to the photon sample and select events with photons in [30, 80] ns window. The extracted photon $E_{\rm T}$ and $\not\!\!E_{\rm T}$ distributions are scaled by $2 \times 3.14/50$ factor.

4.4 Beam Halo

After applying beam halo cuts, we find the remaining background to be less than 1 event, therefore we drop it from the consideration. The technique that used for the background estimation is described in [7]. To recap, the rejections cut is based on the

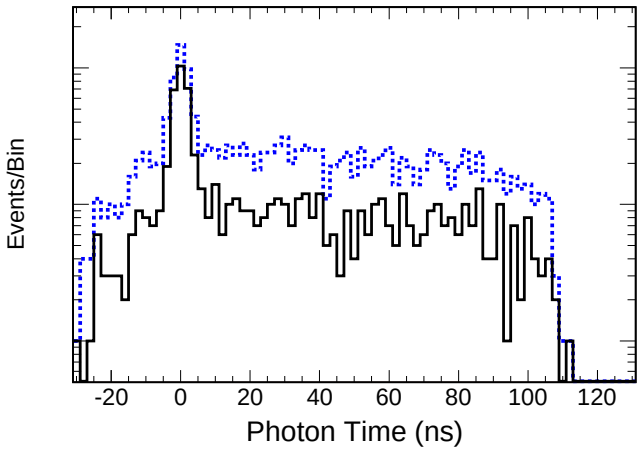

Figure 4: The plot shows by how much cosmic background drops when the requirement to have at least 3 COT tracks is applied.

number of EM central and HAD plug towers with deposited energy along the same wedge as the photon. Most of the beam halo events are concentrated in wedges 0 and 23. To calculate signal efficiency we count how many $W \rightarrow e\nu$ events fail this cut. To estimate the background itself we need to know the rejection power of the cut. To do that we select photons with no underlying collision and remove cosmics from the consideration. Once we know both the efficiency and rejection power it is simple algebra to estimate the remaining background. The cut we use in this analysis defines beam halo as photon plus at least 8 CEM towers plus at least 2 PHA/WHA towers.

5 Signal Efficiency

This section summarizes efficiencies for various cuts applied to the data. The enumeration for the cuts corresponds to the enumerations in Table 1. To derive the efficiencies we use exactly same data that passes exactly the same trigger, only instead of photon we require an electron. Table 3 has all numbers. In order to extract the efficiency for the cut, we apply all other analysis cuts but the current cut and calculate the ratio of events that fails it.

The timing cut efficiency, ϵ^{t0}, is calculated by applying the timing cut to $W \to e\nu$ electrons. This requires an electron to have timing information and to be within timing window. For the second period of data taking the efficiency is independent of $E_{\rm T}$, while for the first period it falls with decreasing energy. For the first period we quote the combination of this cut with the RVM cut.

The RVM discriminant, ϵ^{RVM}, efficiency is independent of $E_{\rm T}$ above 40 GeV. It is true both for the first and the second data sets. For reference, the RVM efficiency for the first data period is at 95%. This makes sense because by requiring the existence of HADTiming information we require a non-zero values of HadE/EmE, the variable used by RVM.

The efficiency of 3 tracks requirement, ϵ^{3t}, is taken from inclusive $W \to e\nu$ sample, where we drop the electron track from consideration. This part is luminosity dependent, and we derive it separately for two data periods.

The efficiency associated with extra collisions arises from events where high $E_{\rm T}$ object other than a photon comes from a different collision. This becomes a factor for the high luminosity data where there are 3 interactions on average for every beam crossing. It is estimated from $W \to e\nu$ electrons by requiring a difference in z between the electron track and jet/track to be greater than 5 cm.

		1569 pb^{-1}	427 pb^{-1}
ϵ^{t0}	timing cut	96.5 ± 1.9	$\epsilon^{HadT}(E_{\rm T})$
ϵ^{RVM}	RVM cut	91.5 ± 2.2	
ϵ^{3t}	at least 3 tracks	79 ± 0.0	47
ϵ^{bh}	beam halo cut	98.6 ± 1.4	same
ϵ^{ec}	extra-collisions	97.9 ± 0.0	100

Table 3: Cut efficiencies, separated for the first and second data taking periods. $\epsilon^{HadT}(E_{\rm T})$ is taken from Figure 3 with SVM part folded in.

6 SM Backgrounds

Most of the backgrounds are estimated using $W \to e\nu$ events selected from W_NOTRACK trigger. The luminosity and the good run selection are identical to the signal data with photons. There is one irreducible background from $Z\gamma$ production when Z decays into two neutrinos. Other significant background is from cosmic rays. It is described in the separate chapter.

6.1 $Z\gamma, Z \to \nu\nu$

The first and most important physics background is irreducible $Z\gamma$ production when the Z boson decays into two neutrinos. We estimate this background from MadGraph Monte Carlo [12] sample. The sample is generated with photons $E_{\rm T} > 20$ GeV and $|\eta| < 2$. The background estimate is

The formula for the background prediction is:

$$N^{50(90)} = \sigma \times \alpha \times (L_1 \times \epsilon_1 + L2 \times \epsilon_2) \tag{1}$$

where $\sigma = 1065$ fb^{-1} is generated cross-section at leading order,
$\alpha = 7402(1871)/99138$ is the acceptance for reconstructed central photons of $E_{\rm T} >$ 50(90) GeV, L_1 and L_2 are the luminosities for two run periods,
and ϵ_1 and ϵ_2 are the other cut efficiencies for two run periods given by Equation 2. The systematic uncertainties are shown in Table 4.

The ratio of NLO cross-section to LO in the presence of the jet veto is shown in Figure 5. We keep the scale factor at 1 and assign a systematic error of 3.5%. We do not rely on Pythia to correctly reproduce jet $E_{\rm T}$ spectrum for this process, therefor we do not have a jet veto cut when $|alpha$ is calculated in Equation 1.

The efficiencies of the additional cuts in the analysis are given by Equation 2 and given in Table 3:

$$\epsilon = \epsilon^{t0} \times \epsilon^{RVM} \times \epsilon^{3t} \times \epsilon^{bh} \times \epsilon^{ec}. \tag{2}$$

where all definitions and numbers are given in Table 3. We take the photon $E_{\rm T}$ and $\not\!\!E_{\rm T}$ shapes from Monte Carlo and normalize to the predicted number of events for $E_{\rm T}>$ 50 GeV. The total systematic error on the prediction is given in Table 4.

6.2 $W \to l\nu, l \to \gamma$

Electrons, taus, and muons all can fake a photon. We estimate this background from data by selecting exactly the same events as we would in data, only requiring electron instead of a photon. Then we weight each event by the electron to photon fake function described in [11]. This portion of the background accounts only for $W \to e\nu$ production. To estimate the number of fake photons from muons and taus we take $W \to e\nu$ result and scale it according to the prescription given in [13].

Source	Syst. (%)
Q^2	1
pdf	5
Jet veto	2.4
k-factor	3.5
ϵ	3.2
Luminosity	6
Total	9.5

Table 4: Systematic uncertainties on $Z\gamma$ prediction

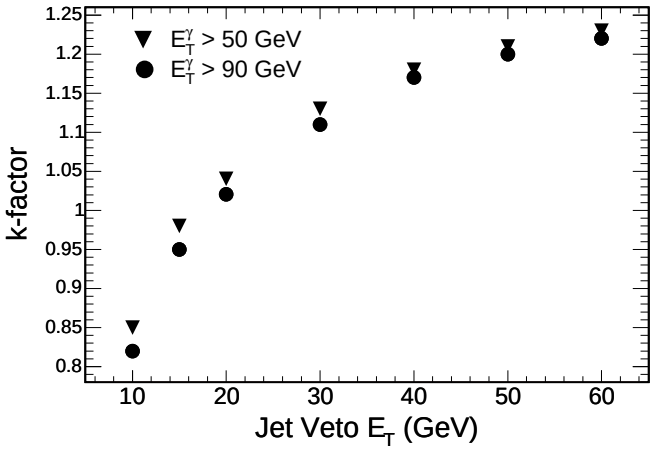

Figure 5: The figure shows the dependence of NLO/LO cross-section k-factor as a function of jet veto cut.

6.3 $W\gamma, W \to l\nu$, lepton is lost

$W\gamma, W \to l\nu$ contributes to the background when the final lepton is simply lost and the resulting signature is a single photon. To estimate $W\gamma$, $W \to e\nu$ we calculate the chance to loose a lepton as a function of a photon E_{T}: $\mathrm{f(E_T)} = \mathrm{MC}^{\gamma+\oslash}/\mathrm{MC}^{\gamma+\mathrm{e}}$. We then scale $\mathrm{f(E_T)}$ to the number of $\gamma + e + \not{E}_{\mathrm{T}}$ events observed in data. Exactly the same procedure is repeated to estimate $W\gamma, W \to \mu\nu$ events when a muon is lost, only instead of an electron in Monte Carlo and data we require a muon.

In the case of $W \to \tau\nu$ the numbers are obtained purely from Monte Carlo. We follow exactly the same steps as for $Z\gamma, Z \to \nu\nu$ background.

6.4 $Z\gamma, Z \to ll$, leptons are lost

The $Z \to ee$ is estimated from Monte Carlo following exactly the same steps as used for $Z\gamma, Z \to \nu\nu$ background. We predict $Z \to \mu\mu$ and $Z \to \tau\tau$ by scaling the above

number by the ratio of events obtained for $W \to l\nu$ modes. It turns out that most of this background comes from lost muons, therefore we do not count this background explicitly to avoid double counting. Since we use data to estimate $W\gamma$ background, all $Z\gamma$ events with one lepton lost would wind up in $W\gamma$ normalization sample.

There is small amount of double counting in $W\gamma$ estimate. Let's say that the probability to loose a track is R. Then the original $Z\gamma$ events would be distributed as $(1-R)(1-R) + 2R(1-R) + R^2$, where the first term is number of events that stays in the sample with two tracks, second term is number of events that ends up in $W\gamma$ sample because one track is lost, and the last term is number of events with both tracks lost. Assuming the probability to loose a track is the same in $W\gamma$ and in $Z\gamma$ is equal to a small value R we have the following. The second term can be approximated by $2R$ in the limit that R is small. Our estimate form Monte Carlo gives for the last term $R^2 = 6$ events. Then $2R^2 = 12$ would propagate into the final sample through the $W\gamma$ data sample. The over-count is equal to $2R^2 - R^2 = 12 - 6 = 6$ events. This number is smaller then the error on $W\gamma$ background, therefor we do not worry about it.

6.5 QCD, γ/jet is lost

QCD $\gamma\gamma$ production contributes to the background when one of the photon is lost is simply lost. To estimate this background we calculate the ratio of single-photon to diphoton events as a function of a remaining photon E_{T}: $\mathrm{f(E_T)} = \mathrm{MC}^{\gamma+\varnothing}/\mathrm{MC}^{\gamma+\gamma}$. We then scale $\mathrm{f(E_T)}$ to the number $\gamma+\gamma$ events observed in data.

We also estimate the background coming from γ + Jet production when the jet is lost or photons is lost and jet fakes photon. The estimate is based purely on QCD γ + Jet Monte Carlo and found to be less than one event. Therefore it is dropped from any considerations.

6.6 Putting It All Together

Full estimation of the total background E_{T} and $\not\!\!E_{\mathrm{T}}$ spectrum are shown on Figure 6. One can see that at low energy there is no dominant background, various pieces contribute on the more or less same footing. As we approach high energies at around 90 GeV, two dominant contributions remain: $Z\gamma, Z \to \nu\nu$ and cosmics, while Electroweak and QCD backgrounds die out. This an *priori* analysis, first we estimated backgrounds, and only after that looked at the data.

Table 5 shows actual breakdown of different backgrounds for two photon energy thresholds. Data agrees with the expectation except one bin at 70 GeV. The total data count is 280 events. The number agrees very well with the background estimate of 264.8 ± 15.2.

We investigate the excess in data in the 70 GeV bin. The χ^2 is $9.2 + 7.2$ for 12 degrees of freedom corresponding to $E_{\mathrm{T}} > 40$ GeV, where the latter χ^2 value is for the bin at 70 GeV. We estimate the significance of the excess due to statistical fluctuation.

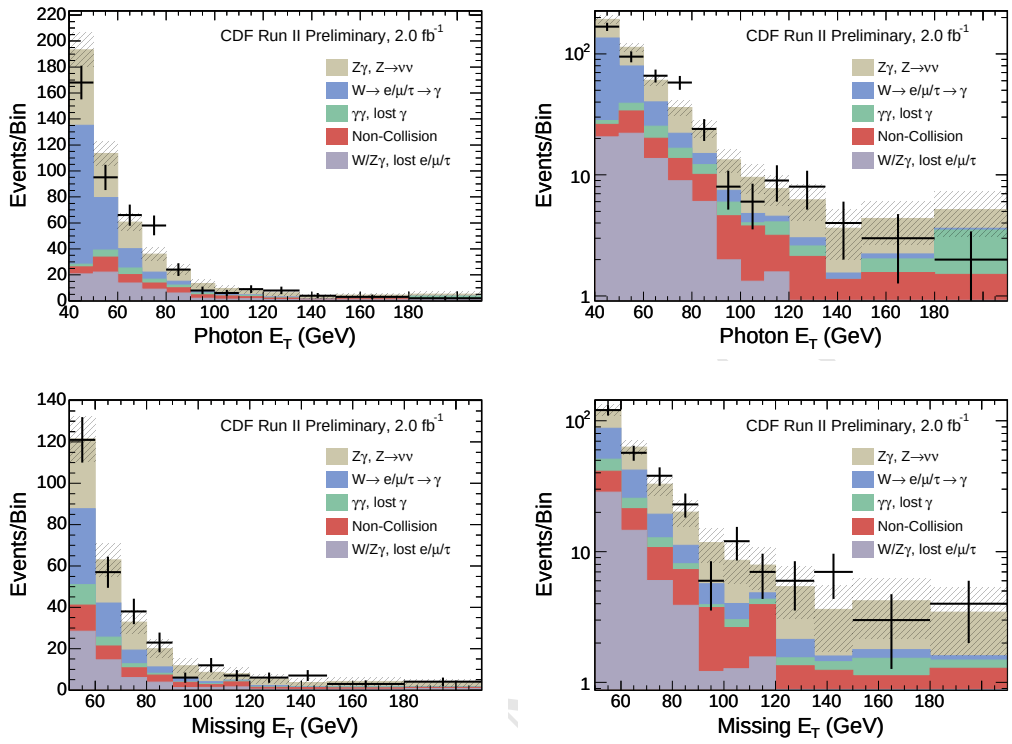

Figure 6: The figure shows photon E_{T} and $\not\!\!E_{\mathrm{T}}$ distributions. The backgrounds are stacked on top of each other.

There are two different methods we use. The first approach is to float each background shape according to the systematic error, and only after that float data according to Poisson. The probability for any bin to have worse χ^2 than 7.2 is 0.68%. In the second approach we float data in each bin using Gaussian around estimated background with statistical and systematic errors added in quadrature. The probability equals to 2.02%. In both cases we arrive to the same conclusion: the significance of the excess is between 2σ and 3σ. Therefore it will be interesting to add more data to the analysis.

Channel	$\gamma E_{\mathrm{T}} > 50$GeV	$\gamma \mathrm{E_T} > 90$GeV
$W \to e \to \gamma$	47.3 ± 5.1	2.6 ± 0.4
$W \to \mu\tau \to \gamma$	19.1 ± 4.2	1.0 ± 0.2
$W\gamma \to \mu\gamma \to \gamma$	33.1 ± 10.2	1.7 ± 1.2
$W\gamma \to e\gamma \to \gamma$	8.0 ± 3.0	0.8 ± 0.7
$W\gamma \to \tau\gamma \to \gamma$	17.6 ± 1.6	2.5 ± 0.2
$\gamma\gamma \to \gamma$	18.9 ± 2.3	2.3 ± 0.6
cosmics	36.4 ± 2.5	9.8 ± 1.3
$Z\gamma \to \nu\nu\gamma$	115.1 ± 9.5	24.8± 2.8
Total	280.5 ± 15.7	46.3 ± 3.0
Data	280	40

Table 5: Background predictions for $\mathrm{E_T} > 50$GeV and $\mathrm{E_T} > 90$GeV for 1996 pb^{-1}.

7 Large Extra Dimensions

One of the models that predicts single photon production in association with heavy particle is LED. We choose this model as a reference point to compare with other experiments and other signatures.

The main process ($q\bar{q} \rightarrow \gamma G_{KK}$) that we target in this analysis is described in [1]. In this type of model extra spatial dimensions are assumed to be compactified with radius R. The model introduces the fundamental mass scale M_D. The two parameters, M_D and R, are related to the Newton's constant and the number of extra dimensions by $G_N^{-1} = 8\pi R^n M_D^{2+n}$. The SM fields propagate only on the normal 3+1 dimensional plane, while gravitons propagate in the bulk, and would appear to us as massive states of the graviton, or, said differently, as massive minimally-interacting particles. Large values of R result in a large phase space for graviton production, canceling the weakness of the coupling to standard model fields. For a given number of extra dimensions the production cross section scales as $1/M_D^{n+2}$. It turns out that the kinematics are independent of M_D for a given n.

We optimize the cut on photon E_{T} to gain maximum sensitivity for the signal from LED using background estimates before looking at the data. Figure 7 shows the total number of events including the estimated signal from LED. For each of the extra dimensions separate Monte Carlo sample is generated at the mass of $\mathrm{G_{KK}}$ at 800 GeV. We find that the acceptance does changes only within 2% as the $\mathrm{G_{KK}}$ goes from 700 to 1600 GeV. Therefore for all calculations we use 800 GeV and assign a relative 2% uncertainty on the acceptance. Our optimization shows that the maximum sensitivity is reached at photon $E_{\mathrm{T}}>$ 90 GeV for all number of extra dimensions. Table 5 shows the breakdown of various backgrounds. The data yields 40 events above 90 GeV, in good agreement with the predicted 42.3.

The data above 90 GeV agrees with the backgrounds, therefore we set limits [14]. Figure 9 shows our limits and compares them to other measurements. Compared to other searches in the same mode our result shows tremendous improvement in the sensitivity. We are comparable in sensitivity with the monojet result for high number of extra dimensions. We note that in the specific model we use the cross-section in the monojet channel is ~ 120 times larger than in the single photon mode.

Source	Syst. (%)
Q^2	2.0
pdf	1.0
Jet veto	4.8
Mass range	2.0
Total	5.7

Table 6: Systematic uncertainties on signal acceptance

N LED	α (%)	σ^{95}_{exp}	σ^{95}_{obs}	M_D^{exp}	M_D^{obs}
2	7.2	116.5	84.7	1000	1080
3	7.2	116.3	84.7	940	1000
4	7.6	110.3	80.4	910	970
5	7.3	113.7	82.7	880	930
6	7.2	115.8	84.4	860	900

Table 7: Acceptance, σ^{95}, and M_D limits for various numbers of extra dimensions. The acceptance is calculated for $M_D = 800$ GeV, relative systematic uncertainty on α is 2%.

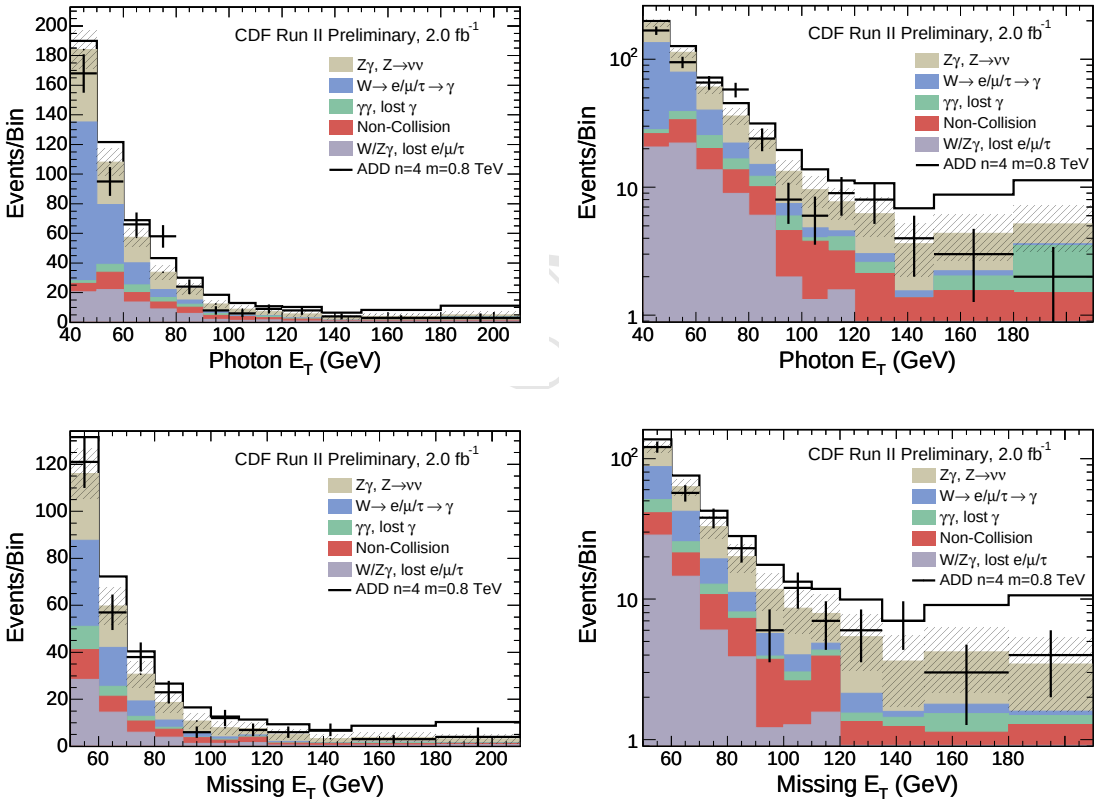

Figure 7: Photon $E_{\rm T}$ and $\not\!\!E_{\rm T}$ distributions with LED signal on top of estimated backgrounds.

8 Combined Limit

We combine our result with the analogous result from exclusive $Jet + \not\!\!E_{\rm T}$ channel. The result is shown on Figure 10. For the combination, we use procedure described in the CDF Note 7587 and the program recommended in this note. The background systematic errors are taken as uncorrelated, while the acceptance systematic errors are

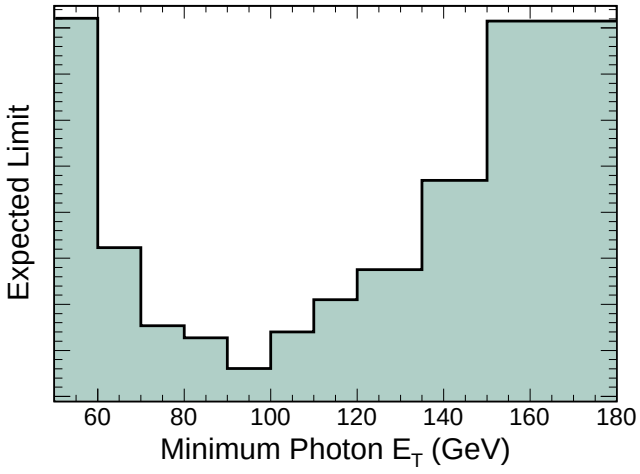

Figure 8: The plot shows the result of the optimization for the LED signal. The best sensitivity is achieved at 90 GeV independent of the extra dimensions.

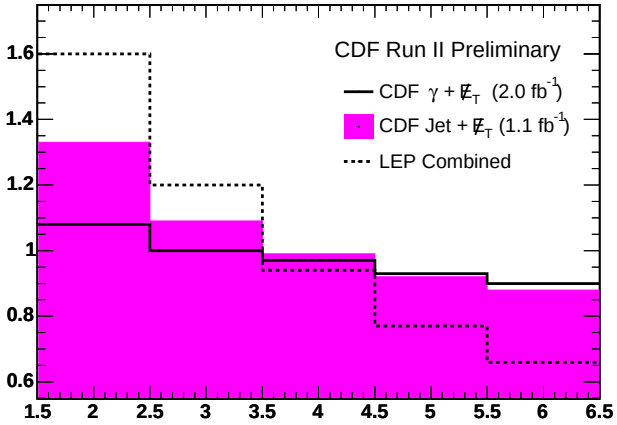

Figure 9: The plot compares the limit with the other best limits on the LED model.

taken 100% correlated between two channels. We use $\gamma + \not\!\!E_{\rm T}$ as a primary channel in the combination, meaning that for the mass extraction we use $\gamma + \not\!\!E_{\rm T}$ LED cross-section curves. The final limits are shown in Table 8.

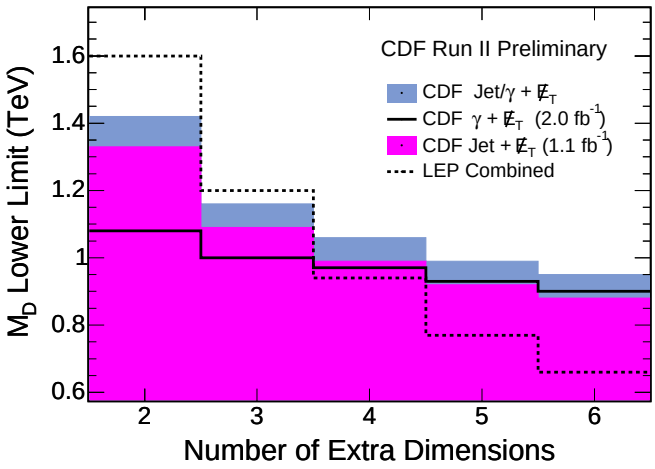

Figure 10: The left plot shows the actual limits on the LED model compared to previous results that used the same search channel. The plot on the right compares the limit with the other best limits on the LED model.

N LED	σ_{obs}^{95} fb	M_D^{obs} GeV
2	26.3	1420
3	38.7	1160
4	46.9	1060
5	52.7	990
6	56.7	950

Table 8: Combined Limits on LED

9 Conclusions

We completed the search for physics beyond the standard model in the single photon channel. We see excellent agreement between the *a priori* estimated background and the data. As a result, we set limits on the Large Extra Dimensions model that are comparable with the best limits from other searches.

We see an excess in data at 70 GeV which is at 2.7 σ level, corresponding to a 0.68% probability for the background to fluctuate up to or above the observed level. It will be interesting to see what happens to the excess when more data is analyzed. If it is not a statistical fluctuation, one possible explanation is that we see the remnants of a 140 GeV resonance with invisible particles produced along with the photons, or with the second photon simply lost in the detector.

10 Acknowledgments

We would like to thank P. Onyisi, H. Frisch, and the rest of the University of Chicago team who completed similar analysis in Run I and the beginning of RUN II and paved the road for the current work. We also would like to thank K. Burkett and E. James for the help to understand LED model and for the help with the code used to generate our LED MC. We would like to thank Tom Junk for providing help and insight into the limit combination procedure.

List of Tables

List of Figures

References

[1] N. Arkani-Hamed, S. Dimopoulos, and G. Dvali, Phys. Lett. B **429**, 263 (1998). 3, 16

[2] Two examples of such models are S. Ambrosanio et al., Phys. Rev. Lett. **76**, 3498 (1996), and B. C. Allanach et al., hep-ph/0112321. 3

[3] K. Burkett, E. James *et al.*, CDF note 8715 3

[4] A. Brignole, F. Feruglio, M. L. Mangano, and F. Zwirner, Nucl. Phys. B **526**, 136 (1998), erratum-ibid. **582**, 759 (2000). 4

[5] http://www-cdf.fnal.gov/internal/physics/photon/docs/cuts.html 4

[6] M.Goncharov *et al.*, *The timing system for the CDF electromagnetic calorimeters*, Nucl.Instrum.Meth. A565, 543 4

[7] M. Goncharov, V.Krutelyov *et al.*, *Discrimination of Beam Halo and Cosmic Rays as a Source of Photon Candidates*, CDF note 8409. 6, 8

[8] Chih-Chung Chang and Chih-Jen Lin, *LIBSVM: a library for support vector machines*, 2001. 6

[9] Helen Hayward, CDF note 7996.

[10] J. Deng, CDF note 7506

[11] R. Culbertson, A. Pronko, Shin-Shan Eiko Yu, CDF note 8220. 11

[12] http://www-cdf.fnal.gov/internal/physics/photon/docs/mclist.html 11

[13] R. Culbertson, A. Pronko, CDF note 8663. 11

[14] J. Heinrich *et al.*, CDF note 7117. 16